Energy & Environmental Science

PAPER

View Article Online
View Journal

Cite this: DOI: 10.1039/c4ee03322a

Semi-transparent perovskite solar cells for tandems with silicon and CIGS†

Colin D. Bailie,‡[a] M. Greyson Christoforo,‡[b] Jonathan P. Mailoa,[c] Andrea R. Bowring,[a] Eva L. Unger,[a] William H. Nguyen,[d] Julian Burschka,§[e] Norman Pellet,[e] Jungwoo Z. Lee,[c] Michael Grätzel,[e] Rommel Noufi,[f] Tonio Buonassisi,[c] Alberto Salleo[a] and Michael D. McGehee*[a]

Received 21st October 2014
Accepted 22nd December 2014

DOI: 10.1039/c4ee03322a

www.rsc.org/ees

A promising approach for upgrading the performance of an established low-bandgap solar technology without adding much cost is to deposit a high bandgap polycrystalline semiconductor on top to make a tandem solar cell. We use a transparent silver nanowire electrode on perovskite solar cells to achieve a semi-transparent device. We place the semi-transparent cell in a mechanically-stacked tandem configuration onto copper indium gallium diselenide (CIGS) and low-quality multicrystalline silicon (Si) to achieve solid-state polycrystalline tandem solar cells with a net improvement in efficiency over the bottom cell alone. This work paves the way for integrating perovskites into a low-cost and high-efficiency (>25%) tandem cell.

Broader context

Hybrid perovskites are a special material for solar cells as they are one of very few efficient high-bandgap absorbers. Furthermore, they can be deposited as defective, polycrystalline layers and are compatible with low temperature and high-volume processing. However, the path to commercialization for this special material is unclear in the current worldwide market. The sharp drop in commercial solar module prices and low profit margins, coupled with high capital intensity for building new solar factories have limited the available investment for new solar technologies. Therefore, an approach that involves upgrading the market-leading technologies is highly attractive, especially if existing factories for these technologies can be leveraged. Mechanically-stacked tandems using hybrid perovskites as the top cell absorber can make use of the entire process flow of current technologies with only the addition of a few steps added in parallel. This approach provides a pathway to commercialization that both provides a benefit for incumbent technologies and does so with low capital intensity.

Introduction

In the last several years the photovoltaic industry has grown rapidly and large factories have achieved superb economies of scale that have enabled the manufacture of modules with power conversion efficiency in the range of 14–21% based on silicon (Si), cadmium telluride (CdTe) and copper indium gallium diselenide (CIGS) at a cost less than $1/W.[1,2] Despite this progress, photovoltaics produce less than one percent of the world's electricity and there is a strong desire to both continue reducing costs to less than $0.5/W while also raising the power conversion efficiency above 25%.[3] Increasing efficiency is particularly important because the cost to install modules now exceeds the cost to make them and the cost of installation effectively drops when the number of panels that needs to be installed to reach a desired power output is reduced. In the last few years, dozens of photovoltaic companies with promising technologies have been forced out of the market.[4] Because new factories require large amounts of capital to build, startups could not achieve the necessary economies of scale to compete in the marketplace with the amount of capital that the investment community was willing to provide. With this in mind, approaches that involve upgrading the market-leading technologies instead of completely displacing them are highly attractive. The power conversion efficiency of silicon photovoltaics has been stuck at 25% for more than fifteen years.[5] We believe that a way to improve on this value is to make tandem solar cells in which a top cell with a higher bandgap than silicon absorbs the higher energy photons and generates a voltage that

[a]Department of Materials Science and Engineering, Stanford University, Stanford, CA 94305, USA. E-mail: mmcgehee@stanford.edu
[b]Department of Electrical Engineering, Stanford University, Stanford, CA 94305, USA
[c]School of Engineering, Massachusetts Institute of Technology, Cambridge, MA 02139, USA
[d]Department of Chemistry, Stanford University, Stanford, CA 94305, USA
[e]Laboratoire de Photoniques et Interfaces, Institut des Sciences et Ingénierie Chimiques, École Polytechnique Fédérale de Lausanne, Station 6, 1015 Lausanne, Switzerland
[f]National Renewable Energy Laboratory, Golden, CO 80401, USA

† Electronic supplementary information (ESI) available. See DOI: 10.1039/c4ee03322a

‡ These authors contributed equally to this work.

§ Current address: Collège des Ingénieurs, Fürstenstrasse 3, 80333 München, Germany.

is approximately twice what silicon can generate. It is desirable to make the high bandgap cell at very low cost using a material than can function well even when it is polycrystalline and defective. Recently, a superb candidate, hybrid perovskites,[6,7] has emerged. Since their first use in photovoltaics in 2009,[8] the power conversion efficiency of polycrystalline thin film perovskite solar cells has soared to over 20%.[5]

The first design principle to consider when making tandem solar cells is choosing the right bandgaps in order to optimize harvesting of the solar spectrum. It is well known that the bottom cell should have a bandgap around 1.1 eV and the top cell should have a bandgap around 1.7–1.8 eV.[9] Si and CIGS both have an ideal bandgap for the bottom cell. In the relatively few cases where tandems were made with Si or CIGS, the top cell sometimes had a bandgap of only 1.4 eV [10] simply because there are relatively few high performing PV materials and one of them, CdTe, has that bandgap. Tandems have also been made with dye-sensitized solar cells, but the efficiency was only 16%.[11]

The perovskite semiconductor most commonly used in solar cells is methylammonium-lead(II)-iodide with the chemical formula $CH_3NH_3PbI_3$ ($MAPbI_3$), which is an inorganic–organic hybrid perovskite that forms a tetragonal crystal structure and is compatible with both solution processing[12] and evaporation techniques.[13,14] $MAPbI_3$ is a strongly absorbing[15] direct bandgap semiconductor[16] with a bandgap around 1.6 eV. In addition, it is an intrinsic material with high carrier mobilities,[17] shallow defect levels,[18] and 1 μm carrier diffusion lengths,[19] which are important metrics for highly performing solar cells. $MAPbI_3$ devices have obtained large open circuit voltages of 1.07 V,[13] only 0.53 V less than the bandgap, E_g/q. The bandgap of the $MAPbI_3$ perovskite (1.6 eV) can be continuously tuned up to 2.25 eV by substituting Br for I to make $MAPb(I_{1-x}Br_x)_3$,[20] which makes perovskite solar cells especially attractive for tandem applications. A simple stoichiometry of 1 : 2 bromine to iodine has the ideal bandgap of 1.76 eV.

A second design principle to consider is how to construct the tandem (Fig. 1). We identify two options that could be used to make practical modules. The classical method is a monolithically integrated tandem (Fig. 1, right). A more unconventional method is a mechanically-stacked tandem (Fig. 1, left). The mechanically-stacked tandem has the advantage of manufacturing simplicity and ease of integration. All commercial photovoltaic modules already contain a glass cover sheet upon which the top cells could be deposited. A mechanically-stacked architecture relaxes performance constraints such as current–density-matching and the need for tunnel junctions while enabling optimization of the top and bottom cells separately. Current matching between the top and bottom strings of cells can be achieved at the module level by adjusting the relative top and bottom cell sizes (Fig. 2). This configuration allows the module to have only two leads exiting the module and requires only a single inverter, similar to conventional single-junction modules. On the other hand, the practical efficiency limit of a monolithic tandem is higher than that of a mechanically-stacked tandem because there are fewer 'transparent' electrodes in the stack that parasitically absorb approximately 5–10% of the light per electrode. However, a monolithic tandem requires the engineering of a tunnel junction or recombination layer, the likely need to planarize the surface of the bottom cell to build the perovskite cell, and photon management within the complicated dielectric stack. In this paper, we demonstrate mechanically-stacked tandems by using a semi-transparent perovskite solar cell as the top cell on

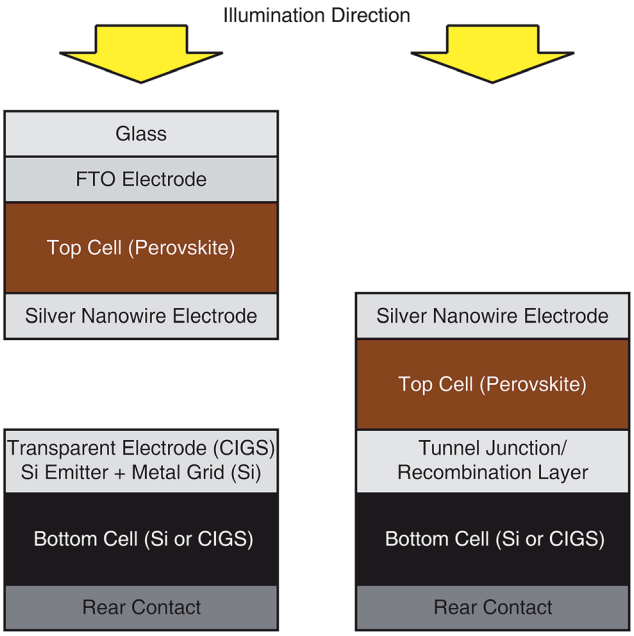

Fig. 1 Tandem schematics. (Left) Schematic of a mechaniically-stacked tandem fabricated in this work with a perovskite solar cell as the top cell and Si or CIGS as the bottom cell. (Right) Schematic of a monolithic polycrystalline tandem.

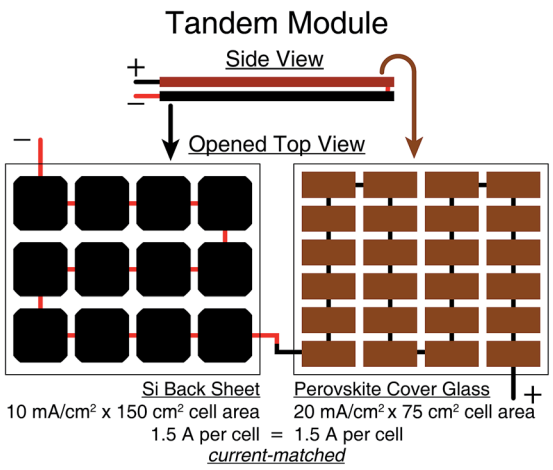

Fig. 2 Current-matching at the module level. An example perovskite/silicon module with a simplified geometry and current density to demonstrate how current-matching at the module level can occur with a mechanically-stacked tandem. In this example module, the filtered silicon produces half the photocurrent density of the perovskite, so the silicon cells are twice as large to match the current of the perovskite cells. In this example, all cells are strung together in series; the total voltage of the module is the sum of the individual cell voltages.

top of Si and CIGS and provide an outlook for the potential of polycrystalline tandems. For this prototype we use previously-developed perovskite, CIGS, and Si solar cells and introduce a new method of depositing a silver-nanowire transparent electrode to enable semi-transparency through the perovskite solar cell.

Results and discussion

Semi-transparent perovskite solar cell

Mechanically-stacked tandems require a semi-transparent top cell, as illustrated in Fig. 1. The perovskite solar cell architecture used in this study is similar to that developed by Burschka *et al.*[12] We use a mesoporous titanium dioxide (TiO_2) layer infiltrated with the perovskite and contacted on either side by electron-selective (compact TiO_2) and hole-selective (2,2′,7,7′-tetrakis(*N*,*N*′-di-*p*-methoxyphenylamine)-9,9′-spirobifluorene, spiro-OMeTAD) contacts (see Experimental section and ESI† for more details). For compatibility with these existing electron- and hole-selective contacts, we use the $MAPbI_3$ perovskite rather than the optically ideal $MAPbBrI_2$. $MAPbBrI_2$ was also not chosen due to a photo-instability observed in this material.[21] The transparent front electrode is fluorine-doped tin oxide (FTO) coated glass. Typically, a perovskite solar cell is opaque with an approximately 100 nm thick metal back electrode of either Au or Ag. This metal back electrode provides a low-resistance electrical contact and a reflective surface, giving the perovskite a second chance to absorb any light that was not absorbed on the first pass. To enable the transparency required to make a mechanically-stacked tandem, we needed a transparent top electrode.

The technical constraints that the top transparent electrode must meet are stringent. The electrode must be highly transparent in the critical 600–1000 nm window where the perovskite is not absorbing all of the light and the bottom cell has significant external quantum efficiency (EQE). The sheet resistance of the transparent electrode should be at most 10 $\Omega\ \square^{-1}$.[22] because the transparent electrode must have high lateral conductivity to minimize resistive loss when carrying the large current density generated in the perovskite cell. Perhaps most importantly, this electrode must be applied after deposition of the spiro-OMeTAD layer onto a temperature- and solvent-sensitive perovskite solar cell without damaging it. For these reasons, high-performance transparent conductive oxides widely used in industry cannot be directly sputtered onto a perovskite solar cell without a buffer layer. An electrode meeting these criteria has not been demonstrated before now. We use a silver nanowire (AgNW) mesh electrode which has been shown in other cases to have a low sheet resistance and high optical transmission[23–26] and develop a new method of depositing this electrode onto our perovskite cell in a room-temperature solvent-free process. This AgNW electrode serves as the linchpin for our mechanically-stacked tandem architecture.

We first form our AgNW transparent electrode on a flexible polyethylene terephthalate (PET) film by spray deposition (see experimental section and ESI†). The resulting AgNW film has a sheet resistance of 12.4 $\Omega\ \square^{-1}$ and exhibits 90% transmission between 530 and 730 nm falling off to 87% at 1000 nm. The AgNW film is then completely and uniformly donated from the PET to the top spiro-OMeTAD layer of the perovskite solar cell by mechanical transfer ideally without damaging the sensitive AgNW or perovskite films (see Experimental section and ESI†). Because this is a research-stage procedure, the applied force of the mechanical transfer was manually rather than automatically controlled. Variability in the applied force can cause shorting (high pressure) as well as incomplete transfer (low pressure), resulting in a spread of device efficiencies (see ESI†). Automated precise control of the applied force is expected to remove these inconsistencies. As a result of the transfer, the conductivity of the AgNW film typically improves by 2 $\Omega\ \square^{-1}$. The primary reason for this increase in conductivity is the planarization of the AgNW film due to the downward force of the transfer lamination process, which reduces the resistance of junctions between wires.[27] A secondary effect is that the AgNWs have been embedded into the moderately conductive spiro-OMeTAD layer ($\sim 10^{-3}$ S cm^{-1})[28] on top of the perovskite device. This transfer step decouples the fabrication of the perovskite solar cell from that of the electrode, allowing each to be optimized independently. Independent fabrication eliminates any thermal or solvent damage that the spiro-OMeTAD or perovskite may otherwise incur during the AgNW deposition process. We complete the semi-transparent solar cell by depositing two lithium fluoride (LiF) anti-reflective (AR) coatings, 133 nm onto the glass surface and 176 nm on top of the AgNW electrode to improve transmission through the device.

The current–voltage curves and metrics of the semi-transparent perovskite cells and opaque control devices are shown in Fig. 3 and Table 1. The loss in absorption in the perovskite due to the removal of the opaque metal back electrode was offset by reduced reflection from the glass surface by the AR coating, yielding comparable J_{sc} between the semi-transparent and opaque cells. We note that if the opaque cell had an AR coating, it would have approximately 0.5 mA cm^{-2} higher photocurrent. We control our measurements for hysteresis in accordance with a paper by Unger *et al.*[29] We found a 5 s delay time between stepping the voltage and measuring current necessary to achieve steady state and remove any semblance of hysteresis. This procedure for removing hysteresis was corroborated and confirmed by NREL when a device was sent for certification. Shadow masks were used to define the illuminated area of a device. Opaque devices were illuminated through a 0.12 cm^2 mask and semi-transparent devices were illuminated through a 0.39 cm^2 mask.

Fig. 3c shows that the transmission through the semi-transparent device peaks at 77% around 800 nm, the center of the 600–1000 nm transmission window that is critical for tandems. Much of the transmission loss is due to parasitic absorption in the FTO electrode, AgNW electrode, and spiro-OMeTAD layer. Uniquely, our semi-transparent device has both a high below-bandgap transmission and a high efficiency. Previous semi-transparent devices have had to sacrifice one of these metrics to achieve the other.[10,23] There remains significant room for improvement in the transmission. Low-temperature processes would allow for fabrication of the perovskite cell on

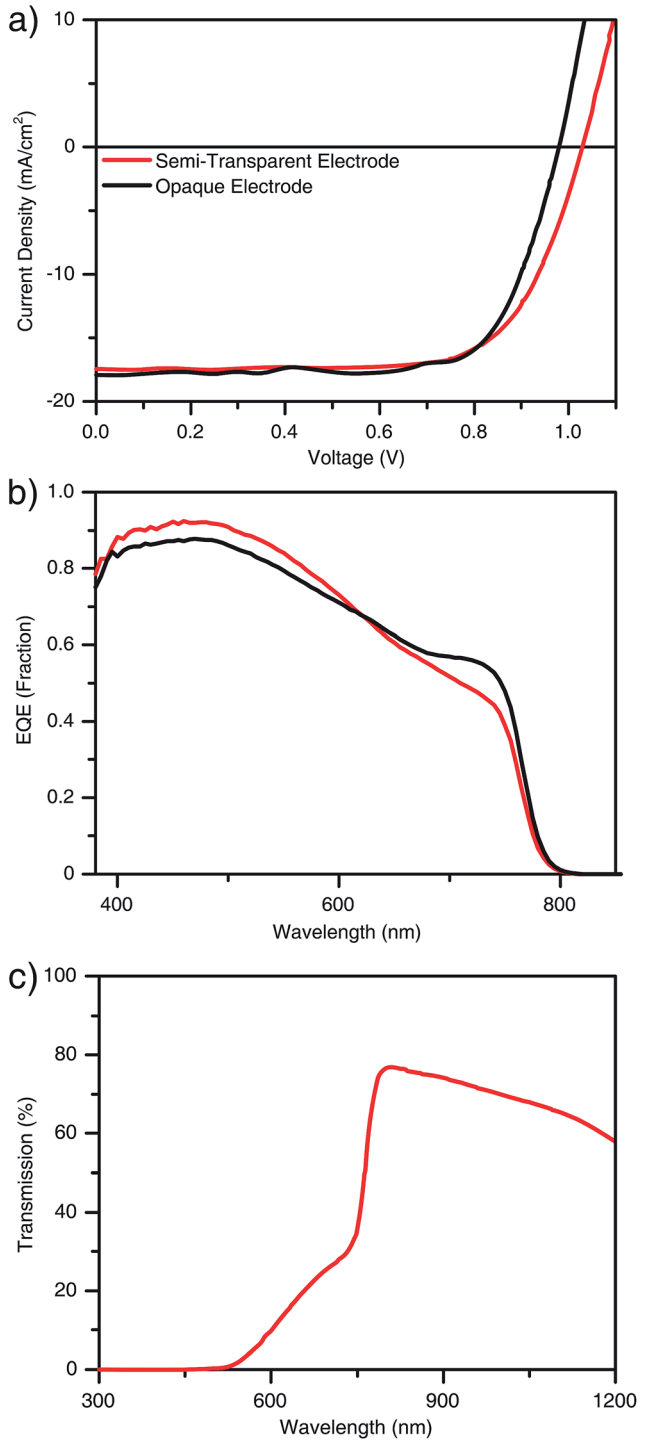

Fig. 3 Perovskite device results. (a) Current–voltage curves comparing best opaque *vs.* semi-transparent perovskite devices. (b) EQE of semi-transparent device and opaque device. Note that the opaque device does not have AR coatings. (c) Transmission through semi-transparent perovskite with AR coatings. Peak transmission is 77% around 800 nm.

ITO, which is more transparent than FTO. A more transparent hole-transporter than spiro-OMeTAD, which in its oxidized form absorbs light throughout the visible and infrared,[28] would also improve transmission.

Table 1 Performance metrics of semi-transparent and opaque perovskite devices

	J_{sc} (mA cm^{-2})	V_{oc} (mV)	FF (—)	Efficiency (%)
Semi-transparent perovskite	17.5	1025	0.710	12.7
Opaque electrode perovskite	17.5	982	0.740	12.7

Tandems

We have made tandems with both Si and CIGS as bottom cells. Both have a bandgap around 1.1 eV, which is sub-optimal for a single-junction solar cell but optimal for a double-junction tandem,[9] and are commercially successful solar technologies. We use a 17.0% laboratory-scale CIGS device made using previously reported procedures.[30–34] Although CIGS cells with 21% efficiency can be made, we chose a cell with a more modest efficiency for this demonstration to illustrate how cells that can be made at scale could be enhanced with a perovskite top cell. The current–voltage curves and external quantum efficiency of the semi-transparent perovskite solar cell, the CIGS solar cell and the CIGS solar cell underneath the perovskite solar cell are shown in Fig. 4. To arrive at the efficiency of the 4-terminal tandem, the efficiency of the semi-transparent perovskite cell is added to the efficiency of the CIGS solar cell when underneath the perovskite cell. With our 12.7% semi-transparent perovskite cell, we improve the 17.0% CIGS cell to 18.6% in a tandem (Fig. 4a and b/Table 2) as measured in-house. This cell was not sent for certification due to scratching of the electrode from excessive handling. A different cell was sent to NREL and was certified as 17.3% with an 11.7% semi-transparent perovskite cell which was slightly higher than our in-house measurement of 17.1% (see ESI† for details). The good agreement between the in-house and certified measurements lends credence to the other values reported herein.

In the perovskite/CIGS tandem, the photocurrent density in the perovskite is 1.6× higher than the photocurrent density in the filtered CIGS. If a module like the one shown in Fig. 2 were made with these two cells, a ratio of 8 perovskite subcells to 5 CIGS subcells (of an area 1.6× the size of the perovskite subcell) should be strung together in series to achieve current matching. We expect that the performance of such a current-matched tandem would be very similar to the 4-terminal values reported here.

Perovskite solar cells are already efficient enough to upgrade the performance of silicon solar cells made with low-quality silicon using the polycrystalline tandem approach. Here, we explore lower-quality sources of Si including cast multicrystalline silicon (mc-Si) wafers made from feedstock with high impurity content recycled from the top 10% of other cast multicrystalline ingots (TI-Si) (Fig. 4c and d/Table 2) and cast mc-Si wafers grown using 4.5 N (99.995% pure) upgraded metallurgical-grade Si (UMG-Si) (see ESI†) instead of the more expensive Siemens-grade polysilicon (9 N, or 99.9999999% pure). Low-quality Si sources generally are not commercially viable today in

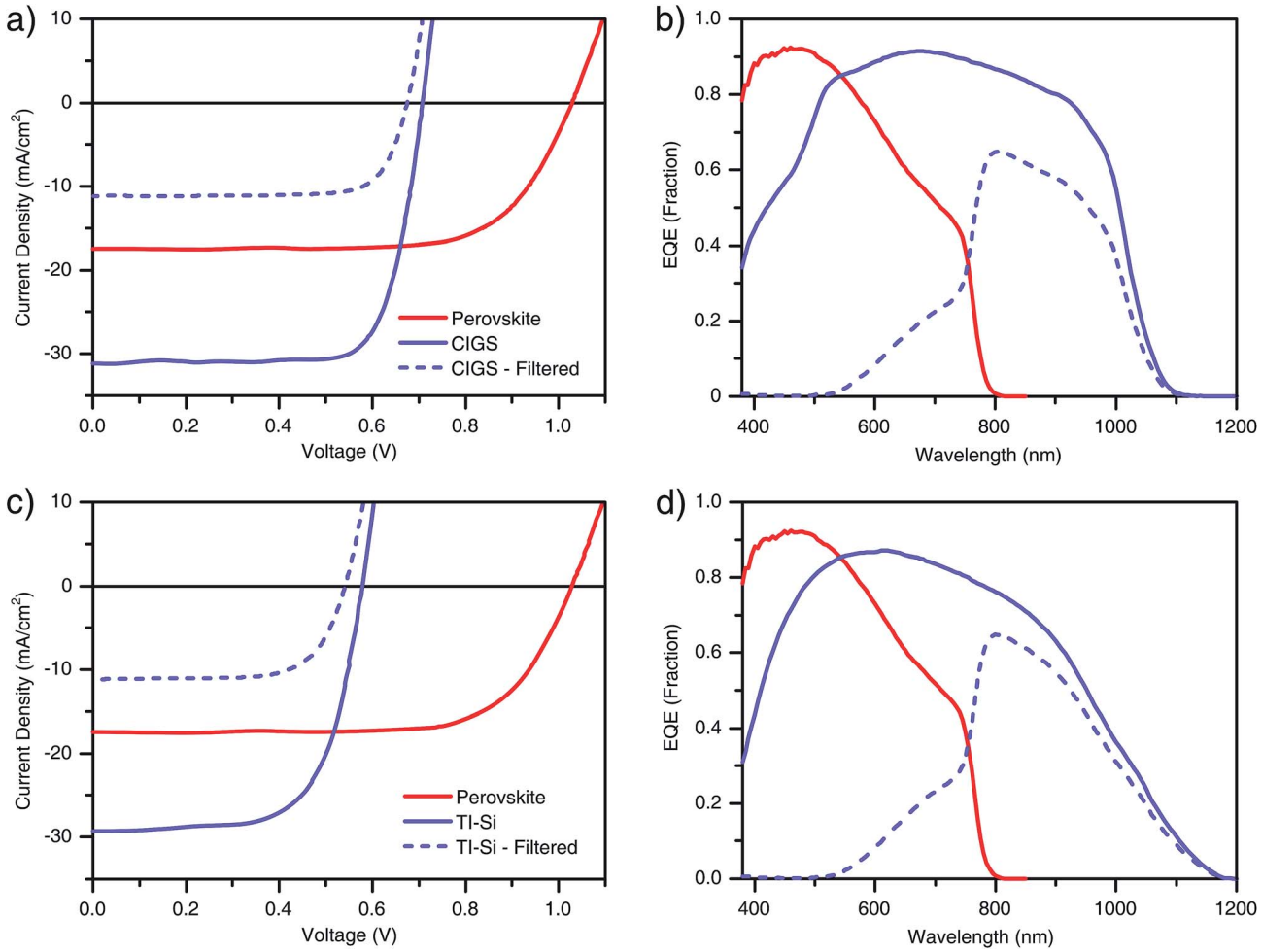

Fig. 4 Perovskite and CIGS/Si tandem results. (a) Current–voltage and (b) EQE of semi-transparent perovskite cell, unfiltered CIGS cell, and CIGS cell filtered by the perovskite cell. (c) *IV* curves and (d) EQE of semi-transparent perovskite cell, unfiltered TI-Si cell, and TI-Si cell with an infrared-optimized anti-reflection coating filtered by the perovskite cell.

Table 2 Performance metrics of semi-transparent perovskite cell, CIGS cell, TI-Si cell, and the resulting tandem efficiencies

	J_{sc} (mA cm^{-2})	V_{oc} (mV)	FF (–)	Efficiency (%)
Semi-transparent perovskite	17.5	1025	0.710	12.7
TI-Si – unfiltered	29.3	582	0.667	**11.4**
TI-Si w/IR-ARC – filtered	11.1	547	0.704	4.3
Tandem w/perovskite + TI-Si				**17.0**
CIGS – unfiltered	31.2	711	0.768	**17.0**
CIGS – filtered	10.9	682	0.788	5.9
Tandem w/perovskite + CIGS				**18.6**

single-junction devices because the material cost advantage of low-quality Si is offset by the reduction in performance due to impurities and crystal defects. We improve an 11.4% low-quality Si cell to 17.0% as a tandem, a remarkable relative efficiency increase of nearly 50%. Such a drastic improvement in efficiency has the potential to redefine the commercial viability of low-quality Si. Another tandem cell was sent to NREL for certification using a 17% silicon bottom cell. The tandem was certified as 17.9% efficient (see ESI† for more details).

When making tandems as opposed to single-junction devices, some design parameters change for the bottom cell. The tandem relaxes the design constraints for both the Si and CIGS top layers. For example, the 20–50 nm CdS window layer used in commercial CIGS devices results in a photocurrent loss of ~0.5 mA cm^{-2} due to reduced EQE from 400–550 nm caused by parasitic light absorption in the CdS layer. However, this does not affect the EQE of a tandem because the 400–550 nm light is already absorbed in the top cell, decoupling the optimization of the electronic and optical properties of the CdS layer. In single-junction Si cells, there is a strict tradeoff of the series resistance *vs.* EQE from 400–550 nm due to minority carrier recombination in the emitter layer. As the bottom cell in a tandem, the emitter thickness or doping can be increased without an EQE penalty. In this work, the Si has a ~35 Ω □$^{-1}$ phosphorus-diffused emitter as opposed to ~100 Ω □$^{-1}$ in industry.[1] Lower sheet resistance in the emitter layer means bus

bar spacing can be increased, reducing shading losses. The design parameters also change for the optimal anti-reflection coatings used in a tandem. All commercial solar cells use AR coatings to improve the transmission into the solar cell. For a single-junction cell, the AR coating on top of the cell is optimized for a broad spectral range from 400–1100 nm and necessarily suffers in performance at the edges of this range. However, for the bottom cell in a tandem, the AR coating is optimized for a much narrower spectral range between 800 and 1100 nm, and can maintain a much higher performance through this narrower spectral range. Full consideration of the different design parameters between single-junctions and tandems such as these examples could yield further improvements in the future.

Outlook of polycrystalline tandems with perovskites

Perovskite solar cells, in both their opaque and semi-transparent versions,[35] are still in their infancy. As perovskite cells continue to improve, tandems employing them will directly benefit from these improvements. We note that the benefit of the tandem instead of a single junction cell is maximized when the top and bottom cells have approximately equivalent single-junction device performance. While we have not yet demonstrated a tandem that can compete directly in efficiency with record single-junction CIGS, Si, or perovskite cells, we estimate that converting the current record perovskite efficiency of 20.1% from an opaque to a semi-transparent cell and coupling it with a 21–22% single-crystal Si solar cell would result in a 25–27% efficient tandem. Before commercialization, issues pertaining to stability, yield, and the use of lead should be addressed. If the lead-based perovskite is found unsuitable for commercialization due to these issues, it may inspire the community to develop a new material that can be used as the high-bandgap semiconductor in a polycrystalline tandem.

To estimate how efficient polycrystalline tandems can practically become, we model the performance of a monolithic tandem by making optimistic, but realistic, assumptions including no parasitic absorption from the window layers (see Experimental section for details). With these assumptions, a perovskite with a bandgap of 1.76 eV achieves current matching. For this bandgap, which corresponds to the $MAPbBrI_2$ perovskite, a photo-stable material must be developed. It is possible the $MAPbBrI_2$ can stabilized or an alternative perovskite material with this bandgap is needed. The tandem with this perovskite bandgap can reach 30.4% efficiency, which agrees with the projected efficiency of other models.[36] Since most, if not all, of the layers in a perovskite cell can be deposited from solution, it might be possible to upgrade conventional solar cells into high-performing tandems with little increase in cost.

Experimental

Perovskite device procedure

After cleaning and patterning FTO glass, a ~50 nm thick film of TiO_2 was deposited by spray pyrolysis followed by immersion in a $TiCl_4$ solution. ~350 nm mesoporous TiO_2 films were spun onto the TiO_2/FTO surface and sintered at 450 °C. The remainder of device fabrication was performed in a nitrogen glovebox with <5 ppm O_2 and H_2O. The TiO_2 substrates were dried and brought into the glovebox. Three solutions were prepared: 1.3 M PbI_2 in anhydrous *N*,*N*-dimethylformamide (DMF), 10 mg MAI per 1 mL anhydrous 2-propanol (IPA), and pure IPA as a rinse solution. Methylammonium iodide (MAI) was synthesized according to a previously reported procedure.[6] These concentrations were chosen to avoid the formation of a perovskite capping layer on top of the mesoporous titania, which results in light scattering and decreased transparency to the bottom cell.

The PbI_2/DMF solution was spun on then dried. Films were dipped in the MAI/IPA solution for approximately 20 min to form the perovskite. After rinsing and drying, a spiro-OMeTAD solution was spun on. Films were removed from the glovebox and stored overnight in a desiccator at 20% relative humidity.

For opaque electrode devices, 100 nm Au was thermally evaporated through a patterned shadow mask to form the back electrode.

For semi-transparent devices, an AgNW film was transferred on top (see following section). 100 nm Ag was thermally evaporated through a patterned shadow mask around 3 edges of the devices. 133 nm LiF was deposited onto the glass surface and 176 nm LiF onto the AgNW mesh.

AgNW electrode procedure

AgNWs were dissolved in methanol and spray deposited from solution with a pneumatic airbrush-type spray nozzle onto flexible Polyethylene terephthalate (PET) film at 60 °C. The volatile alcohol solvent evaporates during the deposition and only AgNWs remain on the PET substrate. This airbrush-type deposition ensures uniformity and repeatability over an arbitrarily large deposition area.

The patterned AgNW film on PET was placed with the AgNWs in contact with the spiro-OMeTAD layer on top of the perovskite device. A 0.17 mm thick glass coverslip was placed on top of the PET substrate. The AgNWs were transfer laminated from the PET to the perovskite solar cell by applying approximately 500 g of downward force onto the coverslip through a single 1/4 inch diameter ball bearing and selectively rolling over the active area of the perovskite.

I–V Measurements

Current–voltage characteristics of the perovskite cells were measured using a Keithley model 2400 digital source meter. The irradiation source was a 300W xenon lamp (Oriel). The lamp was calibrated against the integrated photocurrent obtained by EQE. The voltage was swept in the direction of open circuit to short circuit. A 5 s delay time at each voltage step before taking data removed any transient hysteretic behavior of the perovskite devices.[29] For consistency, Si and CIGS cells were measured with the same sweep parameters.

The semi-transparent perovskite was illuminated through a 0.39 cm^2 aperture area. The total area of the CIGS and Si is also

0.39 cm^2, to minimize leakage current. The opaque perovskite cell was illuminated through an 0.12 cm^2 aperture area.

Tandem measurement method

The EQE of the top cell, bottom cell, and bottom cell filtered by the top cell are individually determined. The solar simulator is calibrated against the expected photocurrent of the cell from the EQE measurement. A *J–V* curve returns the essential metrics of the cell's performance. The procedure is repeated for all three cases. In a 4-terminal configuration, the performance of the individual cells is added together.

Tandem optical model

To model the best-case scenario for a monolithic tandem of perovskite on CIGS, the following assumptions were made:

The AgNW electrode has a 90% transmission with no parasitic absorption from the heterojunction window layers (*e.g.* TiO_2 and spiro-OMeTAD).

For the top cell, 90% EQE with a sharp bandgap was assumed (*i.e.* 90% EQE right up to the edge of the bandgap) with an E_g–V_{oc} gap of 0.4 V and a FF of 0.80.

For the bottom cell, the best-case Si device was modeled in PC1D with the following parameters: 1 cm^2 device area, 300 μm thick p-type wafer with 1.5×10^{16} cm^{-3} background doping, 3 μm rear surface texturing, n^{++} emitter contact with 1×10^{19} cm^{-3} peak doping, p^+ back surface field with 1×10^{18} cm^{-3} peak doping, 1 ms bulk recombination lifetime, front-surface recombination velocity of 10 cm s^{-1}, rear-surface recombination velocity of 1000 cm s^{-1}, electrode series resistance of 0.015 Ω, and no internal shunt pathways.

To estimate the tandem efficiency, the V_{oc} was added from the top and bottom cells and the J_{sc} and FF were chosen as the lower from the two cells.

Competing financial interests

The authors declare no competing financial interests.

Author contributions

C. B. fabricated perovskite solar cells performed IV and EQE measurements. M. C. developed the silver nanowire electrode process and performed computations. J. M. and J. L. made the Si cells. R. N. made the CIGS cells. J. B. and N. P. provided support on making perovskite solar cells. M. W. provided assistance with cost modeling. A. B. modeled the performance of tandems. E. U. advised on experiments and processes and synthesized the MAI compound. W. N. synthesized the spiro-$(TSFI)_2$ compound. C. B. and M.M. wrote the manuscript. M.M., T.B., R.N., A.S, and M.G. directed the project. All authors reviewed and/or edited the manuscript.

Acknowledgements

This work was primarily supported by the Department of Energy through the Bay Area Photovoltaic Consortium under Award Number DE-EE0004946. This material was also based on work supported by the Center for Advanced Molecular Photovoltaics under Award Number KUS-C1-015-21 by the King Abdullah University of Science and Technology (KAUST), and the Global Climate and Energy Project (GCEP). The nanowire electrode fabrication work was performed in part at the Stanford Nanofabrication Facility's nSiL lab, which was funded by National Science Foundation award ARI-0963061. The muticrystalline silicon device fabrication was performed in part at the Harvard Center for Nanoscale Systems, which was funded by National Science Foundation award ECS-0335765. Jonathan P. Mailoa and Jungwoo Z. Lee were supported by the National Research Foundation Singapore through the Singapore MIT Alliance for Research and Technology's Low Energy Electronic Systems research program. A.E. Morishige and J. Hofstetter (MIT) are acknowledged for supplying and advice on preparing the silicon wafers. William H. Nguyen was supported by the Department of Defense (DoD) through the National Defense Science & Engineering Graduate Fellowship (NDSEG) Program. We thank Dmitry Poplavskyy and DuPont for their generous donation of mono-crystalline silicon solar cells. We acknowledge helpful feedback from an anonymous reviewer.

References

1 *International Technology Roadmap for Photovoltaic (ITRPV) 2013 Results*, 2014.
2 M. Osborne, *First Solar hits cost reduction milestone*, PV-Tech, 2013, http://www.pv-tech.org/news/has_first_solar_retaken_the_lowest_cost_pv_manufacturer_mantle.
3 *DOE Technical Report*, 2012, DOE/GO–102012–3037.
4 E. Wesoff, greentechmedia, 2013, http://www.greentechmedia.com/articles/read/Rest-in-Peace-The-List-of-Deceased-Solar-Companies.
5 NREL Efficiency Chart Rev. 12-08-2014, *NREL*.
6 M. M. Lee, J. Teuscher, T. Miyasaka, T. N. Murakami and H. J. Snaith, *Science*, 2012, **338**, 643–647.
7 H.-S. Kim, C.-R. Lee, J.-H. Im, K.-B. Lee, T. Moehl, A. Marchioro, S.-J. Moon, R. Humphry-Baker, J.-H. Yum, J. E. Moser, M. Grätzel and N.-G. Park, *Sci. Rep.*, 2012, **2**, 1–7.
8 A. Kojima, K. Teshima, Y. Shirai and T. Miyasaka, *J. Am. Chem. Soc.*, 2009, **131**, 6050–6051.
9 T. J. Coutts, K. a. Emery and J. Scott Ward, *Prog. Photovoltaics*, 2002, **10**, 195–203.
10 X. Wu, J. Zhou, A. Duda, J. C. Keane, T. a. Gessert, Y. Yan and R. Noufi, *Prog. Photovoltaics*, 2006, **14**, 471–483.
11 P. Liska, K. R. Thampi, M. Grätzel, D. Brémaud, D. Rudmann, H. M. Upadhyaya and a. N. Tiwari, *Appl. Phys. Lett.*, 2006, **88**, 203103.
12 J. Burschka, N. Pellet, S.-J. Moon, R. Humphry-Baker, P. Gao, M. K. Nazeeruddin and M. Grätzel, *Nature*, 2013, **499**, 316–319.
13 M. Liu, M. B. Johnston and H. J. Snaith, *Nature*, 2013, **501**, 395–398.
14 Q. Chen, H. Zhou, Z. Hong, S. Luo, H.-S. Duan, H.-H. Wang, Y. Liu, G. Li and Y. Yang, *J. Am. Chem. Soc.*, 2013, **136**, 622–625.

15 G. Xing, N. Mathews, S. Sun, S. S. Lim, Y. M. Lam, M. Grätzel, S. Mhaisalkar and T. C. Sum, *Science*, 2013, **342**, 344–347.
16 T. Umebayashi, K. Asai, T. Kondo and a. Nakao, *Phys. Rev. B: Condens. Matter Mater. Phys.*, 2003, **67**, 155405.
17 C. C. Stoumpos, C. D. Malliakas and M. G. Kanatzidis, *Inorg. Chem.*, 2013, **52**, 9019–9038.
18 W.-J. Yin, T. Shi and Y. Yan, *Appl. Phys. Lett.*, 2014, **104**, 063903.
19 V. Gonzalez-Pedro, E. J. Juarez-Perez, W.-S. Arsyad, E. M. Barea, F. Fabregat-Santiago, I. Mora-Sero and J. Bisquert, *Nano Lett.*, 2014, **14**, 888–893.
20 J. H. Noh, S. H. Im, J. H. Heo, T. N. Mandal and S. Il Seok, *Nano Lett.*, 2013, **13**, 1764–1769.
21 E. T. Hoke, D. J. Slotcavage, E. R. Dohner, A. R. Bowring, H. I. Karunadasa and M. D. McGehee, *Chem. Sci.*, 2014, **6**, 613–617.
22 M. W. Rowell and M. D. McGehee, *Energy Environ. Sci.*, 2011, **4**, 131.
23 Z. M. Beiley, M. G. Christoforo, P. Gratia, A. R. Bowring, P. Eberspacher, G. Y. Margulis, C. Cabanetos, P. M. Beaujuge, A. Salleo and M. D. McGehee, *Adv. Mater.*, 2013, **25**, 7020–7026.
24 G. Y. Margulis, M. G. Christoforo, D. Lam, Z. M. Beiley, A. R. Bowring, C. D. Bailie, A. Salleo and M. D. McGehee, *Adv. Energy Mater.*, 2013, **3**, 1657–1663.
25 J. Lee, I. Lee, T.-S. Kim and J.-Y. Lee, *Small*, 2013, **9**, 2887–2894.
26 J.-Y. Lee, S. T. Connor, Y. Cui and P. Peumans, *Nano Lett.*, 2008, **8**, 689–692.
27 W. Gaynor, S. Hofmann, M. G. Christoforo, C. Sachse, S. Mehra, A. Salleo, M. D. McGehee, M. C. Gather, B. Lüssem, L. Müller-Meskamp, P. Peumans and K. Leo, *Adv. Mater.*, 2013, **25**, 4006–4013.
28 W. H. Nguyen, C. D. Bailie, E. L. Unger and M. D. Mcgehee, *J. Am. Chem. Soc.*, 2014, **136**, 10996–11001.
29 E. L. Unger, E. T. Hoke, C. D. Bailie, W. H. Nguyen, A. R. Bowring, T. Heumüller, M. G. Christoforo and M. D. McGehee, *Energy Environ. Sci.*, 2014, **7**, 3690–3698.
30 K. Ramanathan, M. a. Contreras, C. L. Perkins, S. Asher, F. S. Hasoon, J. Keane, D. Young, M. Romero, W. Metzger, R. Noufi, J. Ward and A. Duda, *Prog. Photovoltaics*, 2003, **11**, 225–230.
31 M. A. Contreras, B. Egaas, K. Ramanathan, J. Hiltner, A. Swartzlander, F. Hasoon and R. Noufi, *Prog. Photovoltaics*, 1999, **316**, 311–316.
32 R. Noufi, A. M. Gabor, J. R. Tuttle, A. L. Tennant, M. A. Contreras, D. S. Albin and J. J. Carapella, *US Pat.*, US 5,441,897, 15 August 1995; R. Noufi, A. M. Gabor, J. R. Tuttle, A. L. Tennant, M. A. Contreras, D. S. Albin and J. J. Carapella, *US Pat.* US 5,436,204, 25 July 1995.
33 M. A. Contreras, J. Tuttle, A. Gabor, A. Tennant, K. Ramanathan, S. Asher, A. Franz, J. Keane, L. Wang, J. Scofield, and R. Noufi, in *Conference Record of the 24th IEEE Photovoltaics Specialists Conference*, 1994, pp. 68–75.
34 M. A. Contreras, M. J. Romero, B. To, F. Hasoon, R. Noufi, S. Ward and K. Ramanathan, *Thin Solid Films*, 2002, **404**, 204–211.
35 D. Bryant, P. Greenwood, J. Troughton, M. Wijdekop, M. Carnie, M. Davies, K. Wojciechowski, H. J. Snaith, T. Watson and D. Worsley, *Adv. Mater.*, 2014, **26**, 7499–7504.
36 T. White, N. Lal and K. Catchpole, *IEEE J. Photovoltaics*, 2014, **4**, 208–214.

